in the intensity of the flash lamps by dividing by the absorbance of the sample at 235 nm measured on the Cary 219 1 h after the flash, the 1-h interval allowing the aerosol of P_4 to settle. The results are given in Table IV.

It was possible to estimate the pseudo-second-order rate constant for the combination of PH_2 to P_2H_4 (reaction 9) from the rate of formation of P_2H_4. With the assumption that the only reaction PH_2 is recombination of P_2H_4, then at time t

$$(PH_2)_t = 2[(P_2H_4)_\infty - (P_2H_4)_t]$$

For a second-order reaction

$$\frac{1}{(PH_2)_t} - \frac{1}{(PH_2)_{t_0}} = 2k_9(t - t_0)$$

$$(P_2H_4)_t = \frac{A_{t,\lambda}}{\epsilon_\lambda 10}$$

$$(PH_2)_t = \frac{A_{\infty,\lambda} - A_{t,\lambda}}{5\epsilon_\lambda}$$

where $A_{t,\lambda}$ = absorbance of P_2H_4 at λ and time t and ϵ_λ = exctinction coefficient of P_2H_4 at λ.

A plot of $1/(PH_2)_t - 1/(PH_2)_{t_0}$ vs. $t - t_0$ gave a straight line with slope of $2k$. The rate constants were evaluated at 225, 232.5, 235, and 245 nm. The plots were strongly dependent on the A_∞ values which were difficult to measure accurately. A value of $(5.4 \pm 2.4) \times 10^9$ M^{-1} s^{-1} was calculated from the rate constants determined at the above wavelengths.

Quantum Yields. Quantum yields were determined from the product yields and the quanta absorbed on the basis of NH_3 actinometry. The quantum yields for zero time of irradiation were determined from least-squares analyses[34] of quantum yields plotted against time of irradiation (Table V). A value of $\Phi_{PH_3} = 1.65 \pm 0.26$ was calculated by using all the data. If the results in Table V at 5.67 einsteins are omitted, then $\Phi_{PH_3} = 1.78 \pm 0.18$. Values of Φ_{4P_4} of 0.013 ± 0.15 and 0.041 ± 0.156 were calculated from the data with and without the result at 5.67 einsteins, respectively. Initial quantum yield for H_2 is 0.43 ± 0.23 and for P_2H_4 is 0.80 ± 0.08.

Acknowledgment. We thank Dr. John Morimoto for the statistical analysis of the quantum yield data and Professor Robert Strong for the flash photolysis studies. The research was supported by Grant NGR 33-018-148 from NASA.

(34) Burr, I. W. "Applied Statistical Methods"; Academic Press: New York, 1974.

The Molecular Structure of the Cubanelike Compound, $[Mo(NC_6H_4CH_3)(\mu_3\text{-}S)(S_2P(OC_2H_5)_2)]_4$, and a Description of Its Bonding

A. W. Edelblut, K. Folting, J. C. Huffman,* and R. A. D. Wentworth*

Contribution No. 3561 from the Molecular Structure Center and the Department of Chemistry, Indiana University, Bloomington, Indiana 47405. *Received August 28, 1980*

Abstract: The tetramer, $[Mo(NC_6H_4CH_3)(\mu_3\text{-}S)(S_2P(OC_2H_5)_2)]_4$, crystallizes in the triclinic space group $P\bar{1}$ with $a = 24.179$ (5) Å, $b = 14.413$ (3) Å, $c = 12.590$ (3) Å, $\alpha = 75.78$ (1)°, $\beta = 59.65$ (1)°, and $\gamma = 58.35$ (1)° at −170 °C. The structure was solved by using 5893 unique reflections having $F > 2.33\sigma(F)$. Full-matrix, least-squares refinement converged to final residuals of $R_F = 0.085$ and $R_{wF} = 0.070$. The symmetry of the elongated $[MoN(\mu_3\text{-}S)]_4$ moiety is adequately described by the D_{2d} point group. Two Mo–Mo bonds are present. Both Mo–N bond distances and Mo–N–C(aryl) bond angles point to triple-bond character in this linkage. A molecular orbital treatment accounts for the binding of the ligands to the core including four Mo≡N bonds, the metal–metal bonds, and the observed diamagnetism. The molecular orbital treatment is also able to account for the formation of a tetramer when $[MoO(\mu\text{-}S)(S_2CNEt_2)]_2$ is reduced electrochemically.

Cubane-like Fe_4S_4 clusters have become increasingly well-known in recent years.[1] Even more recently, double cubane-like molecules containing two $MoFe_3S_4$ clusters have been obtained and structurally characterized.[2] The isolation of a tetramer of Mo(V), which we have suggested[3] to be $[Mo(N(tol))(\mu_3\text{-}S)(S_2P(OEt)_2)]_4$ (tol = p-$CH_3C_6H_4$) with a cubane-like Mo_4S_4 cluster, is one of the more unusual results from our recent studies of arylimido complexes of molybdenum.[4] Since we made that suggestion, the structure of another tetrameric Mo(V) complex with an authenticated cubane-like Mo_4O_4 cluster, $[MoO(\mu_3\text{-}O)(\mu\text{-}O_2PMe_2)_{1/2}(\mu\text{-}OSPMe_2)_{1/2}]_4$, has also appeared[5] and lends further credence to our original suggestion.

This paper reports the structural characterization of our tetramer and shows that the suggested structure is correct. Moreover, this paper examines the bonding within the tetramer and also accounts in a reasonable fashion for the formation of a tetramer, proposed to be $[MoO(\mu_3\text{-}O)(S_2CNEt_2)]_4^-$, after the reduction of $[MoO(\mu\text{-}O)(S_2CNEt_2)]_2$.[6]

Experimental Section

Crystals of $[Mo(N(tol))(\mu_3\text{-}S)(S_2P(OEt)_2)]_4$ from the original preparation were employed in this structural study. Unit-cell dimensions and

(1) See, for example: (a) Berg, J. M.; Hodgson, K. O.; Holm, R. H. *J. Am. Chem. Soc.* **1979**, *101*, 4586 and references therein. (b) Toan, T.; Teo, B. K.; Ferguson, J. A.; Meyer, T. J.; Dahl, L. F. *Ibid.* **1977**, *99*, 408 and references therein. (c) Bernal, I.; Davis, B. R.; Good, M. L.; Chandra, S. *J. Coord. Chem.* **1972**, *2*, 61.

(2) Wolff, T. E.; Berg, J. M.; Warrick, C.; Hodgson, K. O.; Holm, R. H.; Frankel, R. B. *J. Am. Chem. Soc.* **1978**, *100*, 4630. Wolff, T. E.; Berg, J. M.; Hodgson, K. O.; Frankel, R. B.; Holm, R. H. *Ibid.* **1979**, *101*, 4140. Wolff, T. E.; Berg, J. M.; Power, P. P.; Hodgson, K. O.; Holm, R. H.; Frankel, R. B. *Ibid.* **1979**, *101*, 5454. Wolff, T. E.; Berg, J. M.; Power, P. P.; Hodgson, K. O.; Holm, R. H. *Inorg. Chem.* **1980**, *19*, 430. Wolff, T. E.; Power, P. P.; Frankel, R. B.; Holm, R. H. *J. Am. Chem. Soc.* **1980**, *102*, 4694. Christou, G.; Garner, C. D.; Mabbs, F. E. *Inorg. Chim. Acta* **1978**, *29*, L189. Christou, G.; Garner, C. D.; Mabbs, F. E.; King, T. J. *J. Chem. Soc., Chem. Commun.* **1978**, 740.

(3) Edelblut, A. W.; Wentworth, R. A. D. *Inorg. Chem.* **1980**, *19*, 1110.

(4) (a) Haymore, B. L.; Maatta, E. A.; Wentworth, R. A. D. *J. Am. Chem. Soc.* **1979**, *101*, 2063. (b) Maatta, E. A.; Wentworth, R. A. D. *Inorg. Chem.* **1979**, *18*, 2409. (c) Maatta, E. A.; Haymore, B. L.; Wentworth, R. A. D. *Ibid.* **1980**, *19*, 1055.

(5) Mattes, R.; Muhlsiepen, K. *Z. Naturforsch., B: Anorg. Chem. Org. Chem.* **1980**, *35B*, 265.

(6) De Hayes, L. J.; Faulkner, H. C.; Doub, W. H.; Sawyer, D. T. *Inorg. Chem.* **1975**, *14*, 2110.

0002-7863/81/1503-1927$01.25/0

Table I. Crystal Data for $[Mo(N(tol))(\mu_3\text{-}S)(S_2P(OEt)_2)]_4$

mol formula	$Mo_4S_{12}P_4O_8N_4C_{44}H_{68}$
color of cryst	orange-brown
space group	$P\bar{1}$
unit-cell dimens (at −170 °C; 68 reflections)	
a, Å	24.179 (5)
b, Å	14.413 (3)
c, Å	12.590 (3)
α, deg	75.78 (1)
β, deg	59.65 (1)
γ, deg	58.35 (1)
molecules/cell	2
cell vol, Å^3	3222.11
calcd density, g/cm^3	1.725
mol wt	1673.42
linear abs coeff, cm^{-1}	12.60
cryst dimens, mm	0.07 × 0.16 × 0.12
radiation	Mo Kα (0.710 69 Å) from monochromator
2θ limits, deg	5–45
no. of reflections collected	11777
no. of unique intensities	8519
no. with $F > 0.0$	7234
$F > \sigma(F)$	6661
$F > 2.33\sigma(F)$	5893
final residuals	
R_F	0.085
R_{wF}	0.070
ignorance factor	0.07
goodness of fit	1.32

other information concerning the data collection are given in Table I. Intensity data were collected at −170 ± 4 °C by using a scan speed of 2°/min, a scan width of 2° plus a dispersion correction to allow for the $K\alpha_1/\alpha_2$ split. Stationary 15-s background counts were measured at the extremes of the scan range. Four reflections were chosen as standards and monitored periodically. An examination of the intensities of these reflections indicated no systematic trends in the data. The source–monochromator–sample and the sample-receiving aperture distances were 23.5 and 21.5 cm, respectively. The receiving aperture dimensions were 3.0 mm wide by 4.0 mm high. Complete details concerning the experimental data setup and the low-temperature apparatus as well as the data reduction have been given elsewhere.[7]

The structure was determined by using a combination of direct methods and Fourier techniques. All nonhydrogen atoms were located without difficulty by using an initial data set collected at low temperature with a scan speed of 4°/min.

Due to the large number of variables the full-matrix least-squares refinement was carried out in "blocks". Each block consisted of the Mo_4S_4 core and all atoms connected to a single molybdenum atom. Refinement continued in a cyclic fashion until no significant shifts were observed. All atoms were refined by using anisotropic thermal parameters, and no attempts were made to locate the hydrogen atoms. Several atoms on the periphery of the molecule have large anisotropic thermal motion and four atoms refined to nonpositive definite thermal parameters, as indicated in Table II, which gives the fractional coordinates and the equivalent isotropic thermal parameter.[8] Anisotropic thermal parameters and an ORTEP drawing showing the thermal ellipsoids at 50° probability as well as complete listings of bonded distances and angles and observed and calculated structure factors are available as supplementary material.

The virtual symmetry of the $[MoN(\mu_3\text{-}S)]_4$ moiety was examined by using a previously described[9] version of Nyburg's BMFIT program.[10]

Results and Discussion

The Structure of the Tetramer. The structure of $[Mo(N(tol))(\mu_3\text{-}S)(S_2P(OEt)_2)]_4$ is shown in Figure 1. Bond distances are given in Table III while selected bond angles are given in Tables IV and V, respectively. Bond distances and angles within the dithiophosphate ligands and the metal–ligand chelate rings are comparable to those previously found for $Mo_2O_3(S_2P(OEt)_2)_4$[11]

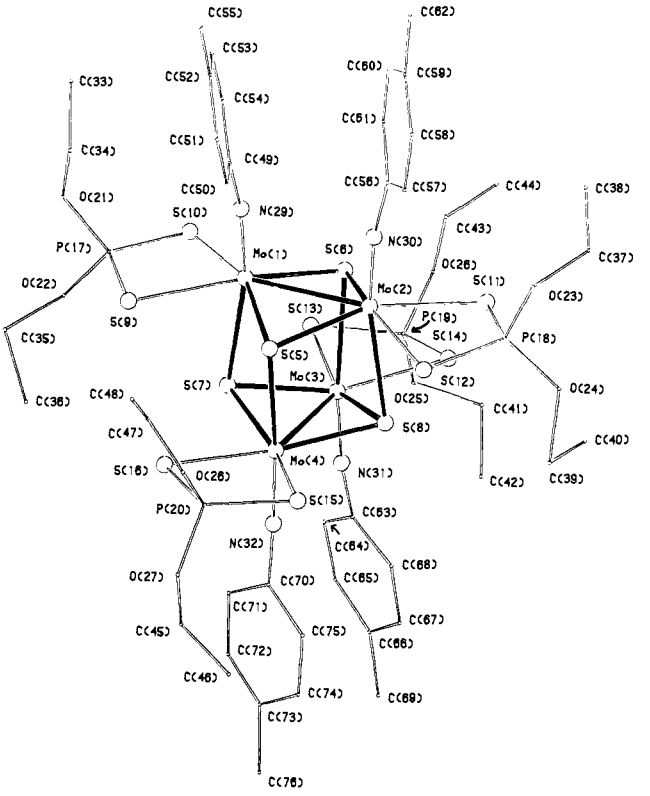

Figure 1. The molecular structure of $[Mo(N(tol))(\mu_3\text{-}S)(S_2P(OEt)_2)]_4$.

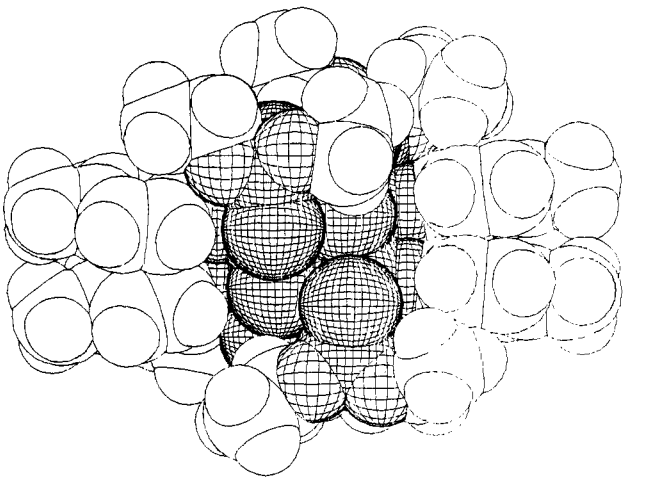

Figure 2. A space-filling model of $[Mo(N(tol))(\mu_3\text{-}S)(S_2P(OEt)_2)]_4$ which clearly shows the arrangement of adjacent aryl rings.

(excluding those distances caused by the trans effect) and $Mo_2O_3(NH)(S_2P(OEt)_2)_2\cdot THF$.[12] Furthermore, distances and angles within the arylimido ligands are close to their expected values while the aryl rings are planar within experimental error. The arrangement of adjacent aryl rings, shown by the space-filling model in Figure 2, is undoubtedly the result of steric interactions between the rings. Our interest in the remainder of the structure concerns the inferences that may be drawn from the magnitudes of the distances and angles within the cubane-like cluster and the Mo–N bond distances and the bond angles subtended at the nitrogen atoms.

The six Mo–Mo distances can be divided into a set of two with distances which are identical within experimental error at 2.862 Å and four with an average distance of 3.69 (±0.04) Å. The former is only slightly longer than the Mo–Mo distance of 2.80

(7) Huffman, J. C.; Lewis, L. N.; Caulton, K. G. *Inorg. Chem.* **1980**, *19*, 2755.
(8) Hamilton, W. C. *Acta Crystallogr.* **1959**, *12*, 609.
(9) Wilson, S. R.; Huffman, J. C. *J. Org. Chem.* **1980**, *45*, 560.
(10) Nyburg, S. C. *Acta Crystallogr., Sect. B* **1974**, *B30*, 251.
(11) Knox, J. R.; Prout, C. K. *Acta Crystallogr., Sect. B* **1969**, *B25*, 1857.
(12) Edelblut, A. W.; Haymore, B. L.; Wentworth, R. A. D. *J. Am. Chem. Soc.* **1978**, *100*, 2250.

Table II. Fractional Coordinates and Isotropic Thermal Parameters[a]

Atom	10^4x	10^4y	10^4z	$10\ B_{iso}$	Atom	10^4x	10^4y	10^4z	$10\ B_{iso}$
Mo(1)	1370(1)	12(1)	5830(1)	17	C(39)	4162(10)	1816(15)	1272(24)	0
Mo(2)	1980(1)	1268(1)	3962(1)	20	C(40)	4450(20)	1205(31)	285(31)	0
Mo(3)	3369(1)	-1576(1)	3961(1)	23	C(41)	5312(12)	-4158(18)	301(18)	69
Mo(4)	2947(1)	-251(1)	5868(1)	20	C(42)	5917(12)	-4376(18)	532(24)	73
S(5)	1621(2)	1295(3)	6091(3)	19	C(43)	3075(12)	-2405(18)	828(18)	55
S(6)	2130(2)	-438(3)	3699(3)	22	C(44)	3194(28)	-2486(26)	-327(35)	237
S(7)	2578(2)	-1538(3)	6080(3)	21	C(45)	3429(8)	291(12)	8614(15)	29
S(8)	3347(2)	119(3)	3744(4)	23	C(46)	3971(9)	738(14)	8041(17)	40
S(9)	809(2)	-138(3)	8167(3)	27	C(47)	904(12)	2529(19)	9206(32)	121
S(10)	1229(2)	-1688(3)	6138(4)	25	C(48)	328(11)	3508(14)	9762(19)	53
S(11)	2745(3)	1220(3)	1643(4)	33	C(49)	-191(7)	1780(10)	6271(12)	15
S(12)	2302(2)	2776(3)	3695(4)	27	C(50)	-388(8)	2754(11)	6747(13)	25
S(13)	3231(2)	-3123(3)	3664(4)	32	C(51)	-1076(7)	3626(11)	7052(14)	25
S(14)	3886(3)	-1646(4)	1634(4)	40	C(52)	-1589(8)	3539(11)	6905(14)	23
S(15)	2885(2)	1483(3)	6236(4)	29	C(53)	-1403(8)	2565(12)	6457(13)	26
S(16)	2226(2)	-1(3)	8188(4)	25	C(54)	-698(7)	1682(12)	6114(13)	24
P(17)	723(3)	-1345(4)	7918(4)	43	C(55)	-2338(8)	4490(12)	7223(16)	37
P(18)	2658(2)	2606(3)	1919(4)	30	C(56)	589(8)	3017(11)	3689(12)	19
P(19)	3888(3)	-3063(4)	1912(4)	40	C(57)	383(8)	4116(11)	3772(14)	25
P(20)	2349(2)	1300(3)	8018(4)	27	C(58)	-258(9)	4925(13)	3679(14)	29
O(21)	-43(9)	-1193(13)	8646(14)	85	C(59)	-667(8)	4649(12)	3483(15)	33
O(22)	1144(7)	-2501(10)	8586(11)	51	C(60)	-444(9)	3538(14)	3392(15)	33
O(23)	2118(6)	3641(8)	1502(10)	35	C(61)	207(9)	2707(12)	3413(14)	29
O(24)	3390(6)	2659(8)	1065(10)	36	C(62)	-1370(9)	5510(14)	3423(16)	42
O(25)	4663(6)	-4089(9)	1573(11)	48	C(63)	495(8)	-3168(12)	3628(15)	32
O(26)	3689(7)	-3265(10)	1012(11)	52	C(64)	5181(9)	-4289(12)	3809(17)	43
O(27)	2721(5)	1214(8)	8797(9)	28	C(65)	5913(10)	-4956(13)	3601(18)	46
O(28)	1610(6)	2343(8)	8660(12)	45	C(66)	6387(10)	-4535(14)	3300(17)	46
N(29)	518(6)	920(9)	5936(11)	25	C(67)	6137(9)	-3402(13)	3066(18)	47
N(30)	1183(7)	2184(9)	3900(11)	25	C(68)	5428(9)	-2727(12)	3228(16)	39
N(31)	4235(6)	-2468(9)	3865(12)	28	C(69)	7169(9)	-5266(16)	3141(21)	0
N(32)	3772(7)	-1097(9)	5909(11)	27	C(70)	4407(7)	-1729(10)	6037(14)	0
C(33)	-713(11)	-95(14)	8698(20)	54	C(71)	4559(9)	-2778(13)	6489(18)	41
C(34)	-1193(18)	-197(21)	8358(22)	91	C(72)	5222(10)	-3405(14)	6544(19)	48
C(35)	986(12)	-2449(15)	9897(20)	62	C(73)	5682(10)	-3017(14)	6265(19)	47
C(36)	1762(15)	-2719(20)	9693(21)	83	C(74)	5499(9)	-1943(14)	5844(19)	45
C(37)	2214(12)	3655(14)	265(16)	50	C(75)	4859(8)	-1277(12)	5748(16)	32
C(38)	1475(11)	4396(16)	315(18)	54	C(76)	6431(11)	6271(15)	6316(25)	74

[a] The isotropic thermal parameters are the isotropic equivalent[8] to those obtained from anisotropic refinement.

(±0.03) Å found in $[MoO(\mu\text{-}S)L]_2$ (L = histidinate,[13] cysteinate,[14] methyl cysteinate,[15] and EDTA[16]), somewhat shorter than the distances of 2.894 Å found[17] in $[MoO(\mu\text{-}S)(\eta^5\text{-}C_5H_5)]_2$ and 2.920 Å found[18] in $[Mo(NCMe_3)(\mu\text{-}S)(\eta^5\text{-}C_5H_5)]_2$, and virtually identical with the average distance of 2.87 (±0.01) Å found[19] for the two isomeric forms of $[MoS(\mu\text{-}S)(S_2C_2H_4)]_2^{2-}$. The 12 Mo–S distances are divided into eight with an average distance of 2.37 (±0.01) Å and four with an average distance of 2.70 (±0.02) Å. The average Mo–S distance in the dinuclear complexes given above is 2.31 (±0.04) Å. The 12 Mo–S–Mo bond angles in the tetramer can be partitioned into four with an average angle of 74.5 (±0.2)° and another eight with an average angle of 93 (±1)°. The 12 S–Mo–S bond angles can also be separated into four with an average angle of 102.0 (±0.1)° and eight with an average angle of 85 (±2)°. The collective evidence points to the presence of the two metal–metal bonds shown in Figure 1.

Each MoS_2Mo bridge containing a metal–metal bond is nonplanar. The dihedral angle between the plane described by S(5), Mo(1), and S(6) and the plane fitting S(5), Mo(2), S(6) is 148° which is identical with the dihedral angle between the planes for S(7), Mo(3), and S(8) and S(7), Mo(4), and S(8). This angle ranges from 145° to 180° in dinuclear complexes containing this bridge.[13-19]

The least-squares plane fitting Mo(1), Mo(2), S(7), and S(8) finds the metal atoms at ±0.023 Å on either side of the plane and the sulfur atoms at ±0.018 Å, while the plane fitting Mo(3), Mo(4), S(5), and S(6) has identical deviations from the plane. The angle between these planes is 89.7°.

The four Mo–N bond distances have an average value of 1.72 (±0.02) Å which is very close to the distance of 1.73 Å established for the Mo≡N linkage in other imido complexes of molybdenum.[4c] The average value of the Mo–N–C bond angle is 171 (±7)°. Bending of this angle between 1 and 8° is common with "linear" MoNR groups, and the additional bending that occurs here is probably the result of the relief of nonbonded contacts in adjacent aryl rings. The average nonbonded distance between adjacent nitrogen atoms is 3.012 (±0.004) Å. The dihedral angle between the least-squares plane fitting Mo(1), Mo(2), S(7), S(8), N(29), and N(30) and that fitting the first four atoms is only 1.3° while the dihedral angle between the plane fitting Mo(3), Mo(4), S(5), S(6), N(31), and N(32) and that fitting the first four atoms is only 0.8°.

Two subsets of distances and angles, related by three mutually perpendicular pseudodiad axes, and the near presence of two mutually perpendicular planes of symmetry indicate that the $[MoN(\mu_3\text{-}S)]_4$ moiety is described approximately by the elements belonging to the D_{2d} point group. Another way to examine the symmetry of this moiety is to use Nyburg's molecular fitting program.[10] This program allows a comparison of the spatial coordinates for the interchange of any group of atoms by a symmetry operation belonging to a point group whose order is greater than that imposed by the crystal. The results for rotations about each of three mutually perpendicular diad axis are shown in Table VI. The relatively minor deviations (Δ) which are observed after these operations as well as the least-squares planes which were discussed above clearly indicate that virtual D_{2d} symmetry is present in this portion of the molecule.

A comparison of the $[Mo(\mu_3\text{-}S)]_4$ cluster in $[Mo(N\text{-}(tol))(\mu_3\text{-}S)(S_2P(OEt)_2)]_4$ with the $[Mo(\mu_3\text{-}O)]_4$ cluster[5] in $[MoO(\mu_3\text{-}O)(\mu\text{-}O_2PMe_2)_{1/2}(\mu\text{-}OSPMe_2)_{1/2}]_4$ indicates that the expected contraction in all distances of the latter has occurred. However, the most unexpected and inexplicable difference in these structures is the bridging nature of the phosphinate ligands in the oxo compound and the normal bidentate nature of the dithiophosphate ligands in the sulfido compound.

Bonding within the Tetramer. A qualitative scheme for the molecular orbitals will be obtained by using idealized D_{2d} sym-

(13) Spivack, B.; Gaughan, A. P.; Dori, Z. *J. Am. Chem. Soc.* **1971**, *93*, 5266.
(14) Brown, D. H.; Jeffreys, J. A. D. *J. Chem. Soc., Dalton Trans.* **1973**, 732.
(15) Drew, M. G. B.; Kay, A. *J. Chem. Soc. A* **1971**, 1851.
(16) Spivack, B.; Dori, Z. *J. Chem. Soc., Dalton Trans.* **1973**, 1173.
(17) Stevenson, D. L.; Dahl, L. F. *J. Am. Chem. Soc.* **1967**, *89*, 3721.
(18) Dahl, L. F.; Frisch, P. D.; Gust, G. R. *J. Less-Common Met.* **1974**, *36*, 255.
(19) Bunzey, G.; Enemark, J. H.; Howie, J. K.; Sawyer, D. T. *J. Am. Chem. Soc.* **1977**, *99*, 4168.

Table III. Bond Distances (Å)

atom	atom	distance	atom	atom	distance
Mo(1)	Mo(2)	2.862 (2)	O(24)	C(39)	1.726 (29)
Mo(1)	S(5)	2.362 (4)	O(25)	C(41)	1.552 (21)
Mo(1)	S(6)	2.370 (4)	O(26)	C(43)	1.439 (23)
Mo(1)	S(7)	2.712 (4)	O(27)	C(45)	1.454 (17)
Mo(1)	S(9)	2.551 (4)	O(28)	C(47)	1.371 (24)
Mo(1)	S(10)	2.558 (4)	N(29)	C(49)	1.396 (16)
Mo(1)	N(29)	1.719 (12)	N(30)	C(56)	1.412 (17)
Mo(2)	S(5)	2.368 (4)	N(31)	C(63)	1.383 (19)
Mo(2)	S(6)	2.372 (4)	N(32)	C(70)	1.388 (17)
Mo(2)	S(8)	2.704 (4)	C(33)	C(34)	1.506 (30)
Mo(2)	S(11)	2.540 (4)	C(35)	C(36)	1.591 (34)
Mo(2)	S(12)	2.569 (4)	C(37)	C(38)	1.502 (26)
Mo(2)	N(30)	1.700 (12)	C(39)	C(40)	1.351 (38)
Mo(3)	Mo(4)	2.861 (2)	C(41)	C(42)	1.492 (32)
Mo(3)	S(6)	2.711 (4)	C(43)	C(44)	1.355 (32)
Mo(3)	S(7)	2.363 (4)	C(45)	C(46)	1.535 (22)
Mo(3)	S(8)	2.367 (4)	C(47)	C(48)	1.363 (26)
Mo(3)	S(13)	2.556 (4)	C(49)	C(50)	1.407 (19)
Mo(3)	S(14)	2.543 (5)	C(49)	C(54)	1.414 (19)
Mo(3)	N(31)	1.745 (12)	C(50)	C(51)	1.376 (19)
Mo(4)	S(5)	2.687 (4)	C(51)	C(52)	1.412 (20)
Mo(4)	S(7)	2.357 (4)	C(52)	C(53)	1.401 (20)
Mo(4)	S(8)	2.366 (4)	C(52)	C(55)	1.501 (20)
Mo(4)	S(15)	2.568 (4)	C(53)	C(54)	1.401 (19)
Mo(4)	S(16)	2.533 (4)	C(56)	C(57)	1.403 (19)
Mo(4)	N(32)	1.729 (13)	C(56)	C(61)	1.418 (20)
S(9)	P(17)	1.970 (6)	C(57)	C(58)	1.413 (20)
S(10)	P(17)	1.975 (6)	C(58)	C(59)	1.380 (22)
S(11)	P(18)	1.997 (6)	C(59)	C(60)	1.411 (22)
S(12)	P(18)	1.976 (6)	C(59)	C(62)	1.518 (21)
S(13)	P(19)	1.976 (6)	C(60)	C(61)	1.401 (21)
S(14)	P(19)	1.985 (6)	C(63)	C(64)	1.406 (20)
S(15)	P(20)	1.979 (6)	C(63)	C(68)	1.413 (22)
S(16)	P(20)	1.993 (6)	C(64)	C(65)	1.412 (24)
P(17)	O(21)	1.507 (15)	C(65)	C(66)	1.416 (25)
P(17)	O(22)	1.708 (13)	C(66)	C(67)	1.424 (22)
P(18)	O(23)	1.571 (11)	C(66)	C(69)	1.534 (24)
P(18)	O(24)	1.573 (11)	C(67)	C(68)	1.387 (23)
P(19)	O(25)	1.573 (12)	C(70)	C(71)	1.396 (20)
P(19)	O(26)	1.568 (14)	C(70)	C(75)	1.406 (20)
P(20)	O(27)	1.582 (10)	C(71)	C(72)	1.397 (23)
P(20)	O(28)	1.558 (11)	C(72)	C(73)	1.355 (24)
O(21)	C(33)	1.545 (22)	C(73)	C(74)	1.409 (23)
O(22)	C(35)	1.507 (23)	C(73)	C(76)	1.571 (23)
O(23)	C(37)	1.450 (19)	C(74)	C(75)	1.381 (21)

Table IV. Bond Angles (Deg) within the $[Mo(\mu_3\text{-}S)]_4$ Cluster

Mo(1)-S(5)-Mo(2)	74.5 (1)	S(5)-Mo(1)-S(6)	102.1 (1)
Mo(1)-S(6)-Mo(2)	74.3 (1)	S(5)-Mo(2)-S(6)	101.9 (1)
Mo(3)-S(7)-Mo(4)	74.6 (1)	S(7)-Mo(3)-S(8)	101.9 (1)
Mo(3)-S(8)-Mo(4)	74.4 (1)	S(7)-Mo(4)-S(8)	102.1 (1)
Mo(1)-S(7)-Mo(3)	93.3 (1)	S(5)-Mo(4)-S(7)	87.0 (1)
Mo(1)-S(7)-Mo(4)	91.9 (1)	S(5)-Mo(4)-S(8)	84.5 (1)
Mo(2)-S(8)-Mo(3)	93.2 (1)	S(6)-Mo(3)-S(7)	85.0 (1)
Mo(2)-S(8)-Mo(4)	93.7 (1)	S(6)-Mo(3)-S(8)	85.7 (1)
Mo(3)-S(6)-Mo(1)	93.2 (1)	S(7)-Mo(1)-S(5)	86.3 (1)
Mo(3)-S(6)-Mo(2)	92.9 (1)	S(7)-Mo(1)-S(6)	84.9 (1)
Mo(4)-S(5)-Mo(1)	92.4 (1)	S(8)-Mo(2)-S(5)	84.1 (1)
Mo(4)-S(5)-Mo(2)	94.1 (1)	S(8)-Mo(2)-S(6)	85.8 (1)

Table V. Additional Selected Bond Angles (Deg)

S(5)-Mo(1)-N(29)	97.1 (4)	S(7)-Mo(1)-N(29)	169.4 (4)
S(6)-Mo(1)-N(29)	104.1 (4)	S(8)-Mo(2)-N(30)	167.5 (4)
S(5)-Mo(2)-N(30)	101.9 (4)	S(6)-Mo(3)-N(31)	168.0 (4)
S(6)-Mo(2)-N(30)	103.4 (4)	S(5)-Mo(4)-N(32)	169.6 (4)
S(7)-Mo(3)-N(31)	103.3 (4)	Mo(1)-N(29)-C(49)	164.7 (10)
S(8)-Mo(3)-N(31)	100.7 (4)	Mo(2)-N(30)-C(56)	170.8 (11)
S(7)-Mo(4)-N(32)	100.4 (4)	Mo(3)-N(31)-C(63)	172.7 (12)
S(8)-Mo(4)-N(32)	101.0 (4)	Mo(4)-N(32)-C(70)	175.0 (11)
S(9)-Mo(1)-S(10)	78.1 (1)	S(13)-Mo(3)-S(14)	78.3 (1)
S(11)-Mo(2)-S(12)	78.2 (1)	S(15)-Mo(4)-S(16)	77.5 (1)

metry. A left-handed coordinate system is imposed on a metal atom with the coordinate axis coincident with the edges of an elongated cube. A right-handed coordinate system is then placed on each donor atom surrounding that metal atom. The remainder of the necessary coordinate systems are related by the S_4 axis. Finally, a left-handed molecular coordinate system is imposed on the elongated cube with the z axis coincident with the direction of elongation and the x and y axes emerging from faces of the cube. While all valence orbitals of the nitrogen atoms of the imido ligands and sulfur atoms within the cluster will be considered, only the σ orbitals of the donor atoms of the dithiophosphate ligands will be included for simplicity.

Table VI. Rotations about Pseudodiad Axes

	rotation defined by (1,2,3,4)[a] →					
	(2,1,4,3)		(4,3,2,1)		(3,4,1,2)	
ref atom	atom	Δ^b	atom	Δ^b	atom	Δ^b
Mo(1)	Mo(2)	0.021	Mo(4)	0.008	Mo(3)	0.016
Mo(2)	Mo(1)	0.021	Mo(3)	0.008	Mo(4)	0.024
Mo(3)	Mo(4)	0.021	Mo(2)	0.008	Mo(1)	0.016
Mo(4)	Mo(3)	0.021	Mo(1)	0.008	Mo(2)	0.024
S(5)	S(6)	0.014	S(7)	0.020	S(8)	0.008
S(6)	S(5)	0.014	S(8)	0.015	S(7)	0.012
S(7)	S(8)	0.023	S(5)	0.020	S(6)	0.012
S(8)	S(7)	0.023	S(6)	0.015	S(5)	0.008
N(29)	N(30)	0.189	N(32)	0.140	N(31)	0.106
N(30)	N(29)	0.189	N(31)	0.103	N(32)	0.084
N(31)	N(32)	0.066	N(30)	0.107	N(29)	0.114
N(32)	N(31)	0.066	N(29)	0.143	N(30)	0.073
$\sum_{i=1}^{8} \Delta^2$		0.003		0.002		0.002

[a] Numbering refers to molybdenum atoms. [b] Distance between original reference atom and shifted atom in Å with least-squares analyses performed only on the $[Mo(\mu_3\text{-}S)]_4$ cluster.

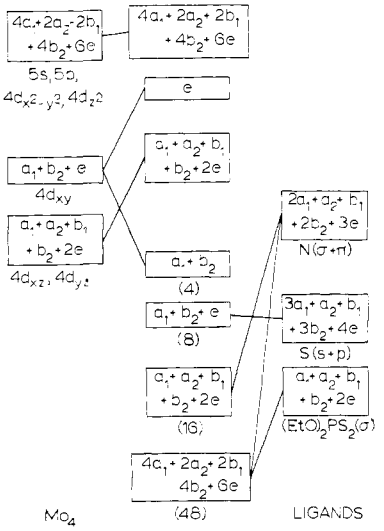

Figure 3. A qualitative molecular orbital diagram for [Mo(N-(tol))(μ_3-S)($S_2P(OEt)_2$)]$_4$ with idealized D_{2d} symmetry. Occupancy of the molecular orbitals is shown by the numbers in parentheses.

The representations which are spanned by these ligand orbitals are shown on the right hand side of Figure 3. Similarly, the representations spanned by the 4d, 5s, and 5p orbitals of the four molybdenum atoms are given on the left-hand side of that figure. When these two sets of representations are compared, it is clear that four relatively nonbonding orbitals on the four sulfur atoms of the cluster must result. These might be considered to be appropriate linear combinations of the 4s orbitals of these atoms. As shown in Figure 3, 32 bonding and 32 antibonding molecular orbitals result from the metal–ligand interactions. Pairwise overlap of the d_{xy} orbitals of adjacent metal atoms on two opposite faces of the cube also results in two bonding molecular orbitals (a_1 + b_2) and a degenerate pair of antibonding orbitals (e). The available 76 electrons then fill the 32 bonding orbitals, the four relatively nonbonding orbitals of the sulfur atoms in the cluster, and the two bonding orbitals resulting from overlap of the metals' d_{xy}

orbitals. The latter account for metal–metal bonds on opposite sides of the cluster.

Although the overlap of the metals' d_{xz} and d_{yz} orbitals will also occur, these orbitals are empty because they are the principal components of molecular orbitals which are strongly antibonding with respect to molybdenum–nitrogen interactions. While the presence of two metal–metal bonds accounts for the shortened metal–metal vectors on opposite faces of the polyhedron, the absence of similar bonding across the other four faces accounts to some extent for the longer distances found on those faces. Consequently, the magnitude of the trans effect exerted by each imido ligand becomes clouded. No trans effect has been found previously with near-linear imido ligands in mononuclear complexes.[4a,c]

The occupied molecular orbitals in Figure 3 account for binding the ligands to the exterior of the cluster including four Mo≡NR groups, intracluster bonding between molybdenum and sulfur atoms, two metal–metal bonds on opposite faces, and the observed diamagnetism.[3] This scheme will also account for bonding within $[MoO(\mu_3\text{-}O)(\mu\text{-}O_2PMe_2)_{1/2}(\mu\text{-}OSPMe)_{1/2}]_4$, providing provision is made for the lone pairs of each terminal oxo ligand. Moreover, the scheme bears some resemblance to those devised by Dahl and his colleagues[1b] for $[Fe(\mu_3\text{-}S)(\eta^5\text{-}C_5H_5)]_4^n$ (n = 1−, 0, 1+, 2+, 3+). Distortions from T_d to D_{2d} or D_2 symmetries, at least with n = 0 and 1+, are apparently due to the Jahn–Teller effect whereas the multiply bound imido ligands are the ultimate reason for distortion within the present $[Mo(\mu_3\text{-}S)]_4$ cluster.

Dimer–Tetramer Equilibria. Although cubane-like tetramers are readily formed in principle from the dinuclear complexes, $[MoX(\mu\text{-}Y)L]_2$ (X = Y = O; X = O, Y = S; or X = Y = S; and L = bidentate ligand), only dinuclear complexes are usually found. We have previously shown[3] that the equilibrium constant for the reaction in eq 1 has a value of 6.3×10^{-4} M^{-1} in dichloroethane.

$$[Mo(N(tol))(\mu\text{-}S)(S_2P(OEt)_2)]_4 \rightleftharpoons 2[Mo(N(tol))(\mu\text{-}S)(S_2P(OEt)_2)]_2 \quad (1)$$

As expected, dilution favors formation of the dimer with a concomitant change in color from red to yellow. Solutions in more polar solvents such as DMF have been found recently to be yellow at all concentrations and devoid of the absorption band due to the tetramer. Bonding between the polar solvent and the dinuclear complex must be energetically more favorable than that afforded by formation of the tetramer in this case. It is undoubtedly true that a very delicate balance of bonding interactions within any of the solvated dinuclear complexes determines their susceptibility to further oligomerization.

However, there is some evidence that the tendency for the formation of tetramers can be enhanced by reduction. The electrochemical reduction[6] of $[MoO(\mu\text{-}S)(S_2CNEt_2)]_2$ in DMF results in the paramagnetic complex, $[MoOS(S_2CNEt_2)]_4^-$, which may have a structure analogous to that of $[Mo(N(tol))(\mu_3\text{-}S)(S_2P(OEt)_2)]_4$. With the assumption that this structure is actually obtained, a closer examination of the antibonding orbitals arising principally from the metals' d_{xy}, d_{xz}, and d_{yz} orbitals is required to explain the enhanced stability of the tetramer after reduction.

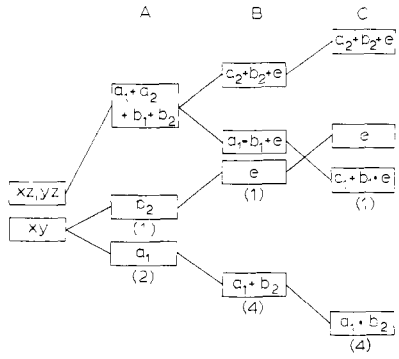

Figure 4. The approximate distribution of some of the bonding and antibonding molecular orbitals for $[MoO(\mu\text{-}S)L]_2^-$ (a) and $[MoO(\mu_3\text{-}S)L]_4^-$ (b and c). The major components of these orbitals are the metals' d_{xy}, d_{xz}, and d_{yz} orbitals. Occupancy of these molecular orbitals is shown by the numbers in parentheses.

An approximate scheme is shown in Figure 4 for these molecular orbitals within the reduced dinuclear complex, $[MoO(\mu\text{-}S)(S_2CNEt_2)]_2^-$, as well as two schemes for a reduced tetramer resulting from the addition of $[MoO(\mu\text{-}S)(S_2CNEt_2)]_2$ to the reduced dimer. The unpaired electron in the reduced dimer should be found in the antibonding b_2 orbital which will result in destabilization. The antibonding $a_1 + a_2 + b_1 + b_2 + 2e$ orbitals which are due to molybdenum–oxygen bonding should be empty. Upon formation of the reduced tetramer, antibonding orbitals from molybdenum–oxygen bonding can be divided into a set of four ($a_1 + b_1 + e$) which remain antibonding with respect to metal–oxygen interactions but are also bonding with respect to metal–metal interactions across the four remaining faces of the polyhedron. Another set of four ($a_2 + b_2 + e$) is antibonding with respect to both types of interactions. If the unpaired electron is found in the antibonding e orbital resulting from overlap of adjacent d_{xy} orbitals, destabilization will be the sole result. If, however, that electron is found in either of the a_1, b_1, or e orbitals which are bonding with respect to additional metal–metal interactions, the total destabilization of the polyhedron will be tempered to some degree by stabilization resulting from additional metal–metal bonds. That stabilization will result because the electron will tend to be delocalized over the four remaining faces of the polyhedron and will increase the number of metal–metal bonds from two to two and half. As a consequence, it is clearly possible that $[MoO(\mu_3\text{-}S)(S_2CNEt_2)]_4^-$ may be more stable than $[MoO(\mu\text{-}S)(S_2CNEt_2)]_2^- + [MoO(\mu\text{-}S)(S_2CNEt_2)_2]_2$ since additional bonding interactions can occur in the former.

Acknowledgment. The authors acknowledge support from the Marshall H. Wrubel Computing Center for the use of computing facilities.

Supplementary Material Available: Listings of all bond angles, observed and calculated structure factors, and anisotropic thermal parameters as well as an ORTEP drawing with thermal ellipsoids at 50% probability are available (85 pages). Ordering information is given on any current masthead page.